

pubs.acs.org/cm Article

# Theory-Driven Spectral Control of Bis-EDOT Arylene Radical Cation Chromophores

Linda Nhon, Simone L. Tennyson, Mason W. Butt, John Bacsa, Aimée L. Tomlinson, and John R. Reynolds\*

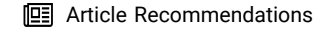


Cite This: Chem. Mater. 2022, 34, 9546-9557



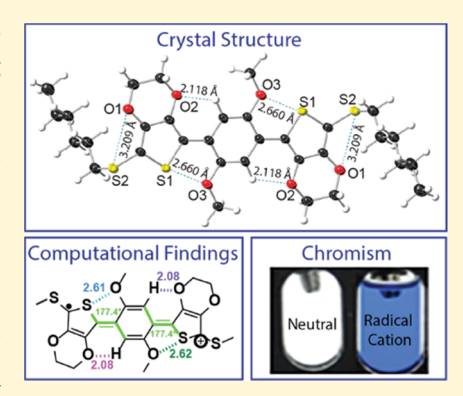
**ACCESS** 

III Metrics & More



Supporting Information

**ABSTRACT:** The electronic structure of  $\pi$ -conjugated materials is responsible for their distinct optoelectronic properties and can be manipulated either by incorporating substituents with varying steric or electronic interactions to influence torsional twist, noncovalent electrostatic interactions, and the degree of electron richness. The structure—property relationship governing the electronic transitions of neutral conjugated molecules is fairly well understood, but this same relationship for the corresponding radical cation/anion has received little attention and the observable transitions can be difficult to predict a priori. Here, we use quantum calculations, specifically density functional theory (DFT) and time-dependent DFT (TD-DFT), to predict how the choice and placement of functional substituents on dioxythiophene-based ter-heterocycles influence the optical properties of the corresponding radical cation and dications states. Specifically, we examine seven thioalkyl-substituted bis(3,4-ethylenedioxythiophene)-1,4-phenylene (BEDOT-B) molecules with varying alkoxy



groups around the central phenylene and compare their optoelectronic, geometric, and excited-state properties by TD-DFT. We then verify the theoretical results with experiments using three model compounds BEDOT-benzene (BEDOT-B), BEDOT-methoxyphenylene (BEDOT-MOB), and BEDOT-2,5-dimethoxyphenylene (BEDOT-2,5-DMOB). Single-crystal X-ray diffraction, ultraviolet—visible (UV—vis) spectroscopy, spectroelectrochemistry, and chemical doping experiments are performed to understand the evolution of the geometric, optical, and electronic properties as the neutral trimers are converted to the radical cation, and to some extent, the dication state. We find that changes in geometric conformation in the radical cations as a result of methoxy substituents are reflected in changes in the dominant high-energy absorbance peak that are associated mainly with the singly occupied molecular orbital (SOMO) having the  $\alpha$  electron spin state transition to the lowest unoccupied molecular orbital (LUMO) having the same electron spin state,  $S_{\alpha} \rightarrow L_{\alpha}$ . However, the low-energy peak associated with the  $S_{\beta} \rightarrow L_{\beta}$  transition remains fairly unaffected by the choice/placement of substituent. Herein, we demonstrate how this observation can be utilized in electrochromic applications as a strategy for fine-tuning the hue and saturation of molecular electrochromes that switch between colorless neutral states and vibrantly colored radical cation states. Fundamentally, this study deepens our understanding of how to synthetically control the optoelectronic properties of conjugated materials in their charged states, guided by TD-DFT to elucidate the electronic transitions at the heart of these properties.

#### ■ INTRODUCTION

Calculations using time-dependent density functional theory (TD-DFT) are becoming an increasingly powerful tool for understanding specific structure—property relationships of discrete molecules, polymers, and other optoelectronic materials. This level of analysis can be done without generating chemical waste, a particularly important aspect during times of supply chain disruptions. Additionally, the computational expenses are much less financially prohibitive than the man-hours that would otherwise be devoted to system generation, characterization, and device formulation. Here, we are employing the TD-DFT model to guide the selection of candidates for developing anodically coloring electrochromic (ACE) molecules, which is a growing class of electrochromes. ACE molecules change from a visibly transparent to a colored

state upon electrochemical oxidation. <sup>12</sup> These materials have potential applications in various technologies such as dimmable eyeglasses, <sup>13</sup> energy-efficient windows, <sup>14–16</sup> and flexible displays. <sup>17–19</sup> Contrary to cathodically coloring electrochromes, <sup>20–23</sup> materials that change color upon electrochemical reduction, ACE molecules are in their nascent development stages. Generally, these are high-energy gap chromophores designed to absorb in the UV region when in

Received: July 8, 2022 Revised: September 28, 2022 Published: October 19, 2022





their neutral state. Upon oxidation, color is induced as they exhibit absorbance peaks that appear in the visible and possibly near-infrared (NIR) region, as illustrated schematically in Figure 1.

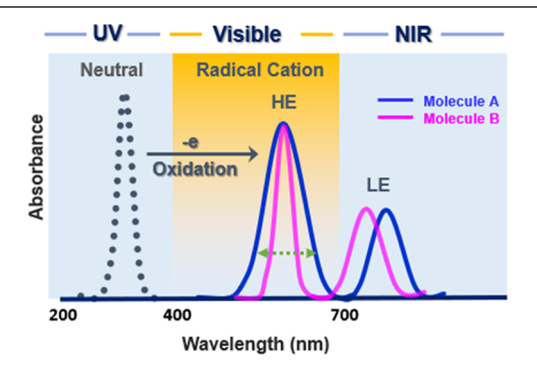


Figure 1. Schematic diagram illustrating the absorption spectra of two ACE molecules with varying steric interactions in their neutral (dotted line) and radical cation (solid lines; A (blue) and B (magenta)) states. In the neutral or uncharged state, both molecules absorb in the UV, and upon oxidation two major absorbance peaks (solid lines) associated with each molecule appear in the visible and near-infrared (NIR) region. In general, the peak in the visible region, often having a higher absorbance intensity than the second band is denoted as the higher-energy (HE) band and the peak in the NIR is considered the lower-energy (LE) band. It is hypothesized that as the molecule becomes more planar with less access to different structural conformations, the width of the HE absorbance band (double-headed green arrow) will vary relative to the degree of conformation. In the schematic, molecule A is less planar than molecule B, hence showing a wider absorbance band, which translates into a lower saturated color state.

In a previous study by Christiansen et al., calculations using TD-DFT elucidated the nature of the excited-state transitions associated with the radical cation absorbance peaks. <sup>12</sup> In that work, a family of ACE chromophores having the structural motif consisting of a 2-thiomethyl-substituted 3,4-ethylenedioxythiophene (EDOT) conjugated to 4-methoxyphenylene derivatives was developed. Electron density was manipulated in this set by adding electron-withdrawing or electron-donating substituents to the phenyl ring's *meta*-position. Quantum calculations on the radical cation revealed that increasing electron richness promotes the low-energy

excited-state transition, from the singularly occupied molecular orbital having the  $\beta$  electron spin state (SOMO $_{\beta}$ ) to the lowest unoccupied molecular orbital (LUMO $_{\beta}$ ), SOMO $_{\beta} \rightarrow$  LUMO $_{\beta}$ , S $_{\beta} \rightarrow$  L $_{\beta}$ . As a result of this transition, Figure 1 shows the second absorbance band pushed into the NIR, leaving a single visible peak. Various colors were assessed in the oxidized states, while the lack of visible light absorption in the neutral state allows these ACE molecules to exhibit high optical contrast.

This work expands on the previous design paradigm by understanding how to manipulate the shape of the radical cation's higher-energy (HE) absorbance independent of the neutral absorbance, which must remain in the UV. Figure 1 illustrates the concepts of two ACE molecules, A and B, sharing a neutral absorbance in the UV (dotted blue line). Upon oxidation, these chromophores exhibit two absorbance curves, where the HE peaks lie in the visible (solid magenta) and the lower-energy (LE) bands extend into the NIR region (solid blue). A single peak in the visible is ideal for accessing one type of color or hue. Furthermore, color saturation can be controlled by manipulating the breadth of the HE band (dotted green arrow).

Herein, we demonstrate how steric interactions can be used to control the width of the charge-state absorbance peak. Using TD-DFT as a guide for synthesis, we examined a set of seven all-donor thioalkyl-substituted bis (3,4ethylenedioxythiophene)phenylene (BEDOT-B) molecules and selected three structures for synthesis. We successfully synthesized and characterized the structure-property relationship of the unsubstituted parent BEDOT-benzene (BEDOT-B), BEDOT-methoxyphenylene (BEDOT-MOB), and BEDOT-2,5-dimethoxyphenylene (BEDOT-2,5-DMOB). In this family, the alkoxy-functionalized phenylene was used to induce varying degrees of intramolecular S···O, O···H, O···O, noncovalent electrostatic interactions.<sup>24</sup> Overall, all three molecules demonstrated ACE properties and exhibited varying degrees of hue and saturation within the blue color space in their oxidized form. The experimental findings strongly agree with the theory; both showed BEDOT-2,5-DMOB having the most promising properties as an ACE molecule that oxidizes at a low potential, exhibits a single narrow radical cation absorbance in the visible region, and has a high electrochromic

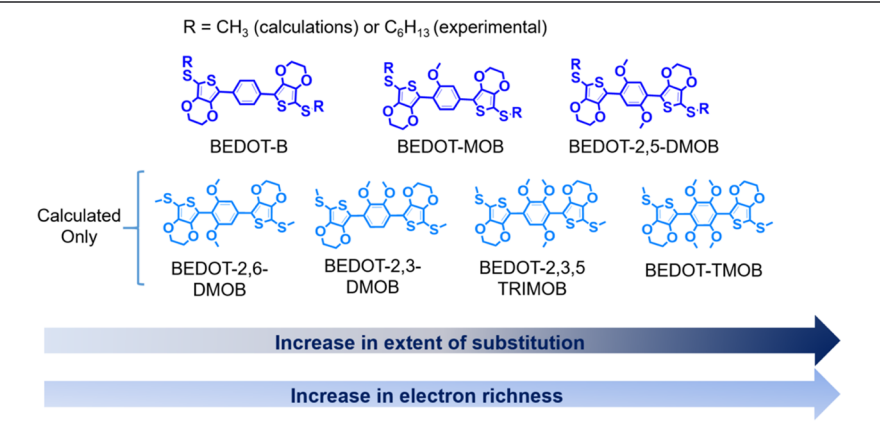


Figure 2. Chemical structures of BEDOT molecules are listed in order of increasing number of methoxy groups and subsequent electron-richness. The top structures show BEDOT-B, BEDOT-MOB, and BEDOT-2,5-DMOB which were synthesized with  $R = C_6H_{13}$  whereas all computations were performed with  $R = CH_{3}$ .

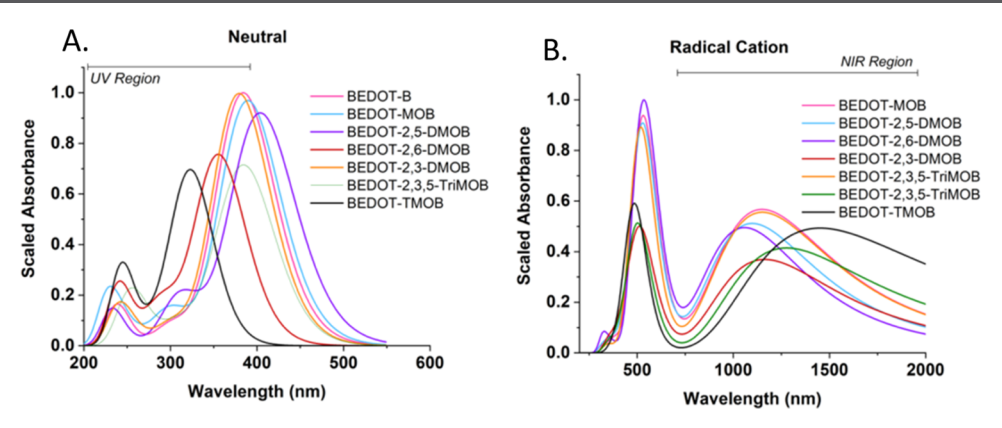


Figure 3. (A) Calculated absorbance spectra of the BEDOT phenylene neutral molecules showing peak isolation in the UV region. (B) Calculated absorbance spectra of the BEDOT phenylene radical cation states showing dual-band absorption in the visible and near-infrared regions.

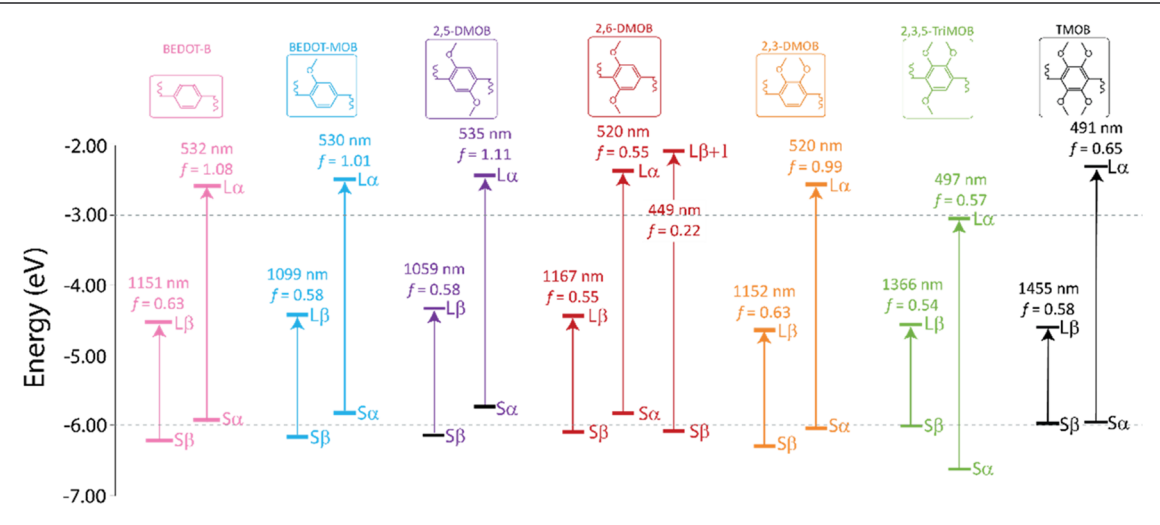


Figure 4. Energy band diagram illustrating the calculated electronic state transitions for the BEDOT phenylene radical cation. All results are reported at the mPW1PBE/cc-PVDZ level with dichloromethane (DCM) inclusion through conductor polarizable continuum model (CPCM).

#### ■ RESULTS AND DISCUSSION

Chromophore Design Rationale. Figure 2 show the seven chemical structures of the family of three-ring  $\pi$ conjugated molecules studied sharing a thioalkyl-substituted BEDOT phenylene core listed in order of increasing electronrich character induced by the number of methoxys. Starting with the least electron-rich BEDOT-B, having an unsubstituted phenylene ring, methoxy groups are incrementally added until all four sites on the phenylene are occupied, as shown by the tetramethoxyphenylene derivative, BEDOT-TMOB. In addition to increasing electron density in the molecular system, the methoxy groups also influence steric and electrostatic interactions. Here, we wanted to compare the **BEDOT-X-DMOB** (where X denotes the site around the ring) isomers and TRIMOB to understand the subtle effects the substituents have on the optoelectronic and geometric properties of both the neutral moleule as well as the radical cation form. The  $\alpha$ -position on the BEDOT has to be protected to prevent coupling of the radical cations, as the terminal 5-positions of the EDOT moieties are expected to have high spin density. We opted to use thioether protecting groups as the sulfur atom is able to donate electron density into the conjugated system, which ultimately facilitates radical cation generation. This thioether motif also allows us to readily modify the end group without affecting the electrochemical or optoelectronic properties as we will show below. To simplify

the TD-DFT calculations, we used a methyl group as the end group for the theoretical predictions, whereas we replaced the methyl group with a hexyl group when synthesizing the model compounds to enhance solubility for ease of purification.

**Excited-State Analysis.** Calculations were conducted on all seven chromophores using DFT and TD-DFT treatments with mPW1PBE functional coupled with the cc-PVDZ basis set with dichloromethane (DCM) inclusion through the conductor polarizable continuum model (CPCM)<sup>25</sup> This model was used to predict their neutral, radical cation, and dication absorbance spectra, along with their excited-state transitions, as summarized in Figure 3, Tables S1, and S2. Figure 3A,B shows the calculated UV—vis spectra generated for both the neutral and radical cation forms. In general, the shapes of the neutral absorbance spectra are similar and are dominated by two major absorption bands and a shoulder. The high-energy (HE) absorption for each molecule is located between 225 and 275 nm and has a lower relative intensity compared to the low-energy (LE) band with maximum absorbance ( $\lambda_{max}$ ) values ranging from 325 nm for BEDOT-TMOB to 404 nm for BEDOT-2,5-DMOB (Figure 3A). These results indicate that these molecules, in their neutral form, mainly absorb in the UV region and are therefore fairly colorless, which we can take advantage of when considering the molecules for electrochromic applications, as will be discussed in more detail in a later section.

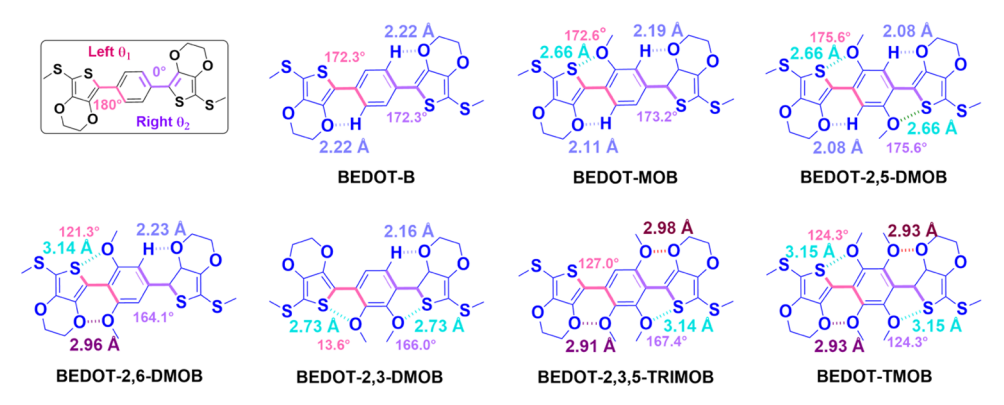


Figure 5. Calculated atomic distances for S···O, O···H, and O···O interactions (Å); dihedral angles (degree) of the BEDOT-X neutral structures. The dihedral angles are provided in pink and purple bold lines both within the structure as well as numerically.

The 15 lowest-lying excited states were utilized to gain insight into the transitions that dominate the neutral-state spectra. From these results, we see that BEDOT-TMOB (and similarly the TRIMOB derivative) has the largest energy gap,  $E_g$  due to its deep HOMO (highest occupied molecular orbital) of -5.88 eV (Figure S1). In contrast, BEDOT-2,5-**DMOB** has the smallest energy gap,  $E_g = 3.07$  eV, and the least negative HOMO at -5.57 eV. These results also demonstrated that the LUMO (lowest unoccupied molecular orbital) only varies by ~440 meV across this set of molecules, whereas the HOMO values vary by ~600 meV, illustrating that the addition of the methoxy groups influences the HOMO value more than the LUMO value, and the variation in electron densities is contributing to the differences observed in the peak positions/ $\lambda_{max}$  values (Figure S1). We were also able to confirm that, in their neutral form, the dominant excited-state transition contributing to their  $\lambda_{max}$  occurs from the HOMO to LUMO, H  $\rightarrow$  L, transition, with strong oscillator strengths (f) ranging from 0.97 to 0.99 across the set (Table S1).

Figure 3B shows the chromophores' calculated radical cation spectra. Each exhibits similar absorbance curves with two distinct absorbance peaks; a HE band centered around 450-550 nm and an LE peak with a  $\lambda_{max}$  that varies from ~1000 to  $\sim$ 1500 nm. The  $\lambda_{\rm max}$  of the HE band appears to be fairly independent of the choice and placement of the substituents  $(\Delta \lambda \sim 40 \text{ nm})$  albeit there are differences in the relative oscillator strength (0.50  $\leq f \leq$  1.00) where BEDOT-B, BEDOT-MOB, and BEDOT-2,5-DMOB have an f near unity and BEDOT-2,6-DMOB exhibits the weakest absorbance with f = 0.50. In contrast, the  $\lambda_{\text{max}}$  of the LE band appears to be much more sensitive to the choice and placement of the methoxy groups as the peak position varies from ~1000 nm out to  $\sim$ 1455 nm with less variance in f. In the absence of measurable quantities like molar absorptivities, the calculated f values are useful since they provide qualitative insight into the light-absorption characteristics of the radical cations, such as which transition(s) will contribute to the dominant absorption peak(s).

Figure 4 shows the energy band diagram for the different radical cations. While the energy band diagram cannot provide information about the width of the peak, it does deliver important insight into the general spectral shape, intensity, and excited-state electronic transitions of the chromophore and allows us to assign the HE and LE bands to specific transitions. The results in Figure 4 reveal that there are two dominant electronic transitions (with f > 0.2) that give rise to the two-band radical cation spectra. First, the dominant process

contributing to the observed HE peak for all seven chromophores is assigned to the transition from the singularly occupied molecular orbital (SOMO) with a one-electron spin-up  $(\alpha)$  state  $(S_{\alpha})$  to the  $L_{\alpha}$ ,  $S_{\alpha} \to L_{\alpha}$ . Second, the LE peak is assigned to the SOMO with a one-electron spin-down  $(\beta)$  state  $(S_{\beta})$  to the  $L_{\beta}$ ,  $S_{\beta} \to L_{\beta}$ . In general,  $S_{\beta}$  orbitals tend to be slightly more stabilized relative to  $S_{\alpha}$ . This difference in energetics results from the SOMO molecular orbital splitting, a phenomenon often observed in odd-electron  $\pi$ -conjugated systems. Moreover, with the exception of BEDOT-2,6-DMOB, the highest f value for each chromophore is associated with the  $S_{\alpha} \to L_{\alpha}$  transition; which explains why the radical cation's HE peak has a higher absorbance intensity than the LE. Further details concerning the various electronic transition states and other photophysical properties are provided in Table

If we compare these results to earlier work by Christiansen et. al who investigated two-ring analogues, there are two important observations. First, the LE band for the radical cation of a two-ring, conjugated 2-thiomethyl-ethylenedioxythiophene conjugated to 4-methoxy-3-cyano-phenylene (ACE1) is dominated by the allowed  $S_{\beta}-1 \rightarrow L_{\beta}$  transition, and second, the peak position is much more blue-shifted with a  $\lambda_{\rm max}$  of 650 nm. This result indicates that by increasing electron richness and extending the  $\pi$ -conjugation, we access the  $S_{\beta} \rightarrow L_{\beta}$  transition, which has a smaller energy gap, while suppressing the the  $S_{\beta}-1 \rightarrow L_{\beta}$  transition. Thus, having control of this type of transition allows us to manipulate where the LE band will appear.

Calculated Geometry: Torsion Angles and Atomic **Distances.** To understand how molecular geometry affects the absorbance spectra, torsional angles and atomic distances were calculated for both the neutral molecule and the radical cation (Tables S4 and S5). The calculated atomic distances can be used to identify various intramolecular steric interactions; for these examples, specifically O···H, O···S, and O···O were observed. The torsional angles, as shown in Figure 5, were also measured from the S-atom on EDOT in an anticonformation to assess the planarity of the system, where 180° is perfectly planar and 90° is contorted out of plane. Figure 5 also shows the chemical structures of the chromophores in the neutral state along with the dihedral angles and atomic distances for O···H (periwinkle), O···O (magenta), and O···S (teal). The torsional angles between EDOT and the phenylene core are represented as  $\theta_1$  (left, pink) and  $\theta_2$  (right, purple) in degrees. To provide a sense for the impact these distances may have on the structure-property relationships, we have compared them

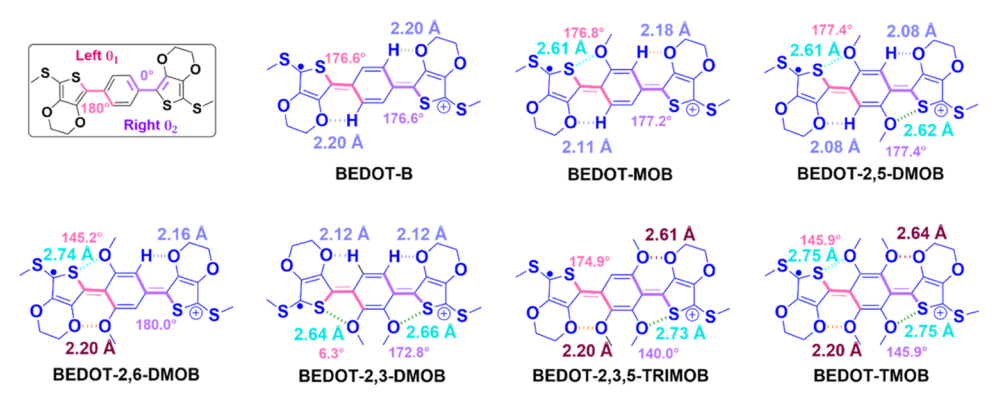


Figure 6. Calculated atomic distances for S···O, O···H, and O···O interactions (Å); dihedral angles (degree) of the BEDOT-X radical cation structures. The dihedral angles are provided in pink and purple bold lines both within the structure as well as numerically.

to the corresponding van der Waals radii [O···O  $\sim$ 2.70, O···H  $\sim$ 2.40, O···S  $\sim$ 3.4 Å].  $^{24}$ 

The torsional angles of BEDOT-B (172°), BEDOT-MOB (173°), and BEDOT-2,5-DMOB (176°) (Figure 5, top row) demonstrate noncovalent interactions induced by either O···H or O···S both of which favor planarity and conformational locking.<sup>24</sup> The proximity of the O-atom to S-atoms affords a larger contribution to planarity than that of the O-atom to Hatoms. However, despite the presence of stabilizing S···O or O...H interactions, BEDOT-2,6-DMOB, BEDOT-TRIMOB, and BEDOT-TMOB (Figure 5, bottom row) also possess repulsive O···O interactions between the methoxy substituents and the oxygen atoms in the dioxybridge of the EDOT. The proximity between adjacent O-atoms induces significant conformational twisting and causes an approximate 50-60° contortion along the S-C-C-C backbone (Figure 5).<sup>24</sup> Additionally, the destabilizing O···O interactions appear to override the stabilization provided by those of the same-side O···S as demonstrated in BEDOT-2,6-DMOB and BEDOT-2,3,5-TRIMOB. These observations suggest that in the absence of O···O repulsions, O···S and O···H interactions planarize the molecules.

These same calculations were conducted on the radical cation structures to elucidate geometric properties. Figure 6 illustrates similar geometric trends in the radical cations analogues. The shorter O···S and O···O atomic distances, as well as smaller torsional angles were calculated for the radical cations indicating they are more planar than the neutral molecules. This finding is further corroborated by comparing the van der Waals distances, which are shorter for a more planar configuration. For example, the most twisted neutral molecule with the largest S-C-C-C torsional angles, BEDOT-TMOB, contorts out of plane by 56°, whereas the corresponding value for its radical cation form is reduced to 34°. This substantial difference between the two forms also occurs in BEDOT-2,6-DMOB and BEDOT-2,3,5-TRIMOB. However, less significant torsional changes occur in the remaining four chromophores (BEDOT-B, BEDOT-MOB, BEDOT-2,5-DMOB, and BEDOT-2,3-DMOB) when converting to the radical cation form, providing further support that the presence of the O···O repulsion results in a larger modification of the molecule's structural conformation.

Another means of comparison is the reorganization energy (RE) which is the structural relaxation a system undergoes upon the gain or loss of an electron. The RE consists of an inner component, which corresponds to changes in intramolecular geometries ( $\lambda_{\rm int}$ ), and an outer component,  $\lambda_{\rm out}$ 

which is related to the solvent response. Given the system and solvent molecules cannot be quantum mechanically calculated together, only the inner component has been determined.<sup>29</sup> The  $\lambda_{int}$  is the sum of both radical cation ( $\lambda^+$  or  $\lambda_{hole}$ ) and radical anion ( $\lambda^-$  or  $\lambda_{\text{electron}}$ ) relaxation; however, only  $\lambda^+$  will be discussed as the focus of this work is centered on radical cations. All three  $(\lambda^+, \lambda^-, \lambda_{int})$  energies have been computed and are given in the SI on page 112. The  $\lambda^+$  is computed using the four-point approach,  $^{30}$  or  $\lambda^{+} = (E_{0}^{+} - E_{+}) + (E_{+}^{0} - E_{0})$ . The  $E_0^+$  refers to the energy which is the result of applying a +1 charge to the optimized neutral geometry and the  $E_{+}^{0}$  is determined by applying a 0 charge to the optimized radical cation geometry. The  $E_0$  and  $E_+$  refer to the energy of the optimized neutral and radical cation geometries, respectively. The lower  $\lambda^+$  the smaller the change between the neutral and charged states the more suitable the system is for use as a charge transfer material. The smallest  $\lambda^+$  values were produced by BEDOT-2,3-DMOB (0.66 eV) < BEDOT-2,5-DMOB (0.72 eV) < BEDOT-MOB (0.77 eV) < BEDOT-B(0.79 eV), and the three remaining systems had  $\lambda^+$  values of 0.96 and higher.

In summary, the geometric analysis provides insight into the types of noncovalent interactions that favor planarity, as well as demonstrates the complexity of understanding how O···O repulsions influence torsional twist. If conformational locking and planarity are considered, then based on the calculated geometric analysis of both the neutral and radical cation forms, BEDOT-B, BEDOT-MOB, and BEDOT-2,5-DMOB are the most planar chromophores in this family. This structural feature may also contribute to their high f values observed in the simulated spectra of the radical cation, which translates to materials exhibiting vibrant colors.

**Selection and Synthesis of BEDOT-X Chromophores.** To verify the accuracy of the TD-DFT calculations on the spectral properties of both the radical cation and the neutral molecules, we selected three of the seven molecules to serve as model compounds for further synthesis and characterization. We ranked this set of structures based on their ability to function as clear-to-colored switching electrochromes due to their vibrant colors, ease of oxidation, and electrochemical stability. Specifically, priority is given to molecules that absorb entirely in the UV region in their neutral state and exhibit a narrow absorption with a high f value in the radical cation state as these criteria are expected to result in the most vibrant color. Also, their structural geometries are utilized in which the degree of planarity, shorter O···H and O···S distances as well as longer O···O separations were considered most desirable.

Based on the spectral analysis in Figure 3, all of the chromophores have their LE peaks in the NIR region of the spectrum, and one observable HE absorbance band in the visible which will contribute to the color of the molecule. As shown in Figure 3A, all seven molecules absorb mainly in the UV, while some tailing into the visible can expected for the most planar molecules. Additionally, from Figure 3B, the oscillator strength of the  $S_{\alpha} \to L_{\alpha}$  transition will greatly impact the hue and saturation of the radical cation absorption as well as determine the degree of color/spectral modulation that will be observed. Taking all of these analyses into consideration, the most promising systems were BEDOT-2,5-DMOB, BEDOT-MOB, and BEDOT-B. These three displayed the most intense radical cation HE peak, the most desirable geometric analyses, and are expected to afford the largest absorption modulation. As such, they were synthesized as a new proof-of-concept for anodically coloring electrochromes (ACE) (see synthetic route given in Scheme 1).

## Scheme 1. Synthetic Route toward BEDOT-B, BEDOT-MOB, and BEDOT-2,5-DMOB

Conveniently, these three molecules were synthesized using identical straightforward Stille cross-coupling conditions. A trimethyl(5-hexylthio)-3,4-ethylenedioxythiophene-2-stannane, was coupled to a commercially available brominated-phenylene (synthetic procedures are provided in the Supporting Information). The EDOT precursor was synthesized in a two-step lithiation reaction using *n*-butyllithium (*n*-BuLi) (Scheme S1). Starting with a nonsubstituted 3,4-ethylenedioxythiophene and utilizing dihexyldisulfide as the electrophile, the hexyl thioether side chain was installed at the 2position resulting in compound 1. While calculations were conducted on the methyl derivatives as a means to conserve computing power, the hexyl side chains were installed to induce organic solubility for ease in the purification process. Then, taking advantage of the capped 2-position, a stannyl group was attached at the 5-position via a second lithiation reaction using trimethyl tin chloride as the electrophile, giving compound 2 in high yield, 82%. Finally, as shown in Scheme 1, the functionalized EDOT was coupled to various dibrominated

phenylene precursors under common Pd-catalyzed conditions, using  $Pd_2(dba)_3$  and  $P(o\text{-tol})_3$  as the catalyst/ligand pair in dimethyl formaldehyde, to yield the final molecules in moderate yields; **BEDOT-B** (52%), **BEDOT-MOB** (43%), and **BEDOT-2,5-DMOB** (47%).

**Structural Analysis.** To confirm the geometry calculations discussed in Figures 5 and 6, the hexyl thioether-substituted BEDOT-MOB and BEDOT-2,5-DMOB were analyzed using single-crystal X-ray diffraction (SC-XRD) as this allows us to examine the torsional angles and bond lengths in the conjugated systems. The crystal structure of a highly similar molecule (highly similar to BEDOT-B) was previously reported by our group and served as a reference molecule for the structural analysis.<sup>33</sup> The differences between these two structures are small and only lie in the presence or absence of the side chain and do not interfere with the parameters of interest here. Suitable crystals of BEDOT-MOB and BEDOT-2,5-DMOB were crystallized from ethanol, yielding fine yellow needles and plates, respectively. Figure 7 shows the perspective

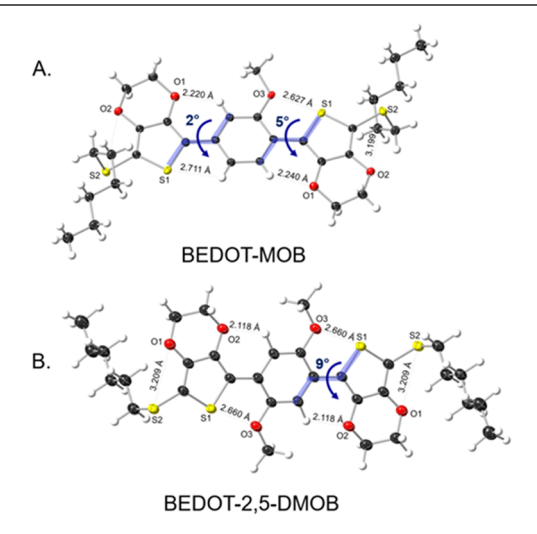


**Figure 7.** X-ray crystal structures of (A) BEDOT-MOB and (B) BEDOT-2,5-DMOB. Selected atoms, O···H and O···S bond distances, and torsion angles are shown.

views of their core structures, where the views are approximately perpendicular to the molecular plane. Atom labels, selected bond distances, and torsional angles are also shown.

The two thiophene rings in BEDOT-MOB are perfectly coplanar. They are also almost coplanar with respect to the central phenyl ring with the central bond, S-C-C-C, having a torsion angle of  $2^{\circ}$  on the nonsubstituted side and  $5^{\circ}$  on the methoxy side (Figure 7A). Similarly, the two thiophene and phenyl ring plane-to-plane twist angles are 3.95(1) and 3.97(1)°, indicating a nearly planar system. The interatomic distance between the phenyl hydrogen and the oxygen from the ethylene bridge is 2.240(2) Å showing that O···H stabilization is occurring in BEDOT-MOB, as theory also predicted.<sup>24</sup> Moreover, a significantly shorter O···S bond distance than its typical bond length (2.637(4) Å), is also observed between the thienyl sulfur atom, S1, and the methoxy oxygen, O(3) (Figure 7A). The large difference between this interatomic distance and the difference between optimal van der Waals radii of ~0.6 Å (van der Waals-observed values), indicates that this interaction is significantly shorter than a

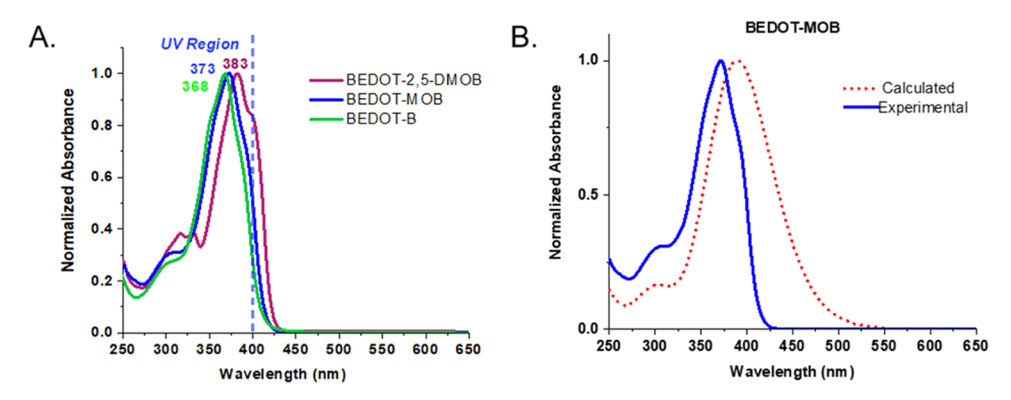


Figure 8. (A) UV—vis neutral absorbance of BEDOT-2,5-DMOB, BEDOT-MOB, and BEDOT-B, taken in dichloromethane. (B) Experimental neutral absorbance spectrum of BEDOT-MOB shows strong agreement with the calculated spectrum.

typical O···S interaction, which suggests an attractive O···S interaction is indeed present. In contrast, a smaller difference of 0.2 Å is observed for the O···H distance. This discrepancy suggests that, for these systems, the O···S interaction will strongly influence the geometry of the molecule, and its strong, attractive force might be the source of the co-planarity. This observation was also validated by theoretical calculations. Overall, the experimental data reduced some of the uncertainty observed earlier in understanding the degree of influence the O···H and O···S interaction have on driving planar conformations.

The **BEDOT-B** is slightly twisted, with an approximate torsion angle of  $\sim$ 28° between the phenylene and EDOT arylrings, <sup>34</sup> likely due to a steric interaction occurring between the phenylene hydrogen and the sulfur atom on the EDOT. Although the experimental torsional strain of 28° along the S–C–C–C backbone is greater than that calculated (S–C–C–C (calculated) = 172°, i.e., S–C–C–C (X-ray comparison) = 8°), **BEDOT-B** is still a relatively planar molecule within this set.

The torsion angle differences between the calculated and X-ray values for BEDOT-MOB and BEDOT-2,5-DMOB are 2 and 5°, respectively. These small differences further validate the computational results. Moreover, the planarity trends are also similar to their calculated values, where BEDOT-B > BEDOT-MOB > BEDOT-2,5-DMOB, which will aid in providing an explanation for the optical properties discussed below.

Finally, these electrostatic interactions and small torsion angles suggest that the methoxy group in BEDOT-MOB aids in driving the molecule toward planarity, supporting our conformational locking hypothesis. Similar observations are made for BEDOT-2,5-DMOB, which is also near-planar with only a 9° torsion angle between the phenylene and EDOT (Figure 7B). The other para-methoxy group provides two O··· S and two O···H interactions in the symmetric molecule. These experimental observations validate the calculations conducted for the neutral molecule's atomic distances and torsion angles. For example, BEDOT-2,5-DMOB calculated O...S differs from the experimental measurement by only 0.01 Å. Like the measurements in the crystal structures, the calculated values for O···H also varied (ranging from 2.20 to 2.08 Å) between the three molecules. These comparisons show that the TD-DFT calculations conducted on these chromophore sets provide reliable insight into the electrostatic interactions and structural conformations of these molecules.

**Neutral-State Absorbance Properties.** The neutral absorbance spectra for the three chromophores taken in dichloromethane, as shown in Figure 8A, are similar in shape, and each has a  $\lambda_{\rm max}$  corresponding to the  $\pi$ - $\pi^*$  high-energy transition that lies within the UV region: BEDOT-B (368 nm), BEDOT-MOB (373 nm), and BEDOT-2,5-DMOB (383 nm). The  $\lambda_{\rm max}$  values of BEDOT-B and BEDOT-2,5-DMOB differ by 20 nm, with the more electron-rich molecule having the more red-shifted absorbance. This shift may be due to BEDOT-2-,5-DMOB's increased electron density, as shown in Figure S1. These chromophores share similar molar extinction coefficients (Figure S2) ranging between 15,000 and 16,000  ${\rm M}^{-1}{\rm cm}^{-1}$  at their respective  $\lambda_{\rm max}$ . Table S1 summarizes the calculated and experimental optical properties for BEDOT-B, BEDOT-MOB, and BEDOT-2,5-DMOB.

Using BEDOT-MOB as an example, Figure 8B shows the calculated and experimental absorbance peaks for the neutral state. The substantial overlap between the two peaks highlights the strong agreement between the predicted spectrum and experimental observation. Only a minor difference of ~10 nm between the calculated and experimental  $\lambda_{max}$  values is observed. This trend is consistent across the experimental set (Figure S3). We find that the  $\lambda_{onset}$  values for the calculated spectra were ~100 nm red-shifted relative to the observed values, which is expected as the overapproximation results from simulation limitations. The deviation in the UV-vis calculations is often attributed to the Gaussian distribution fit around the lower-energy excitation wavelength due to a large deviation from the width of the peak (see Figure 8B).<sup>25</sup> The majority of the neutral absorbance lies in the UV region, thus appearing transparent, which is a desirable property for these ACE systems.

Electrochemical Properties of Oxidized Species. The solution electrochemistry of the chromophores was carried out under an inert Ar atmosphere using 0.5 M tetrabutylammonium hexafluorophosphate (TBAPF<sub>6</sub>) in dichloromethane (DCM) as the supporting electrolyte. A Pt button was used as the working electrode, Ag/AgCl as the reference electrode, and a Pt flag as the counter electrode (Figure S4). Two electrochemically reversible oxidation peaks are observed by cyclic voltammetry (CV) and differential pulse voltammetry (DPV) scans for each molecule, indicating that the radical cation and dication states are accessible under these conditions (Figure S4A). All three molecules oxidize at low potentials, ranging between 0.5 V (BEDOT-B) and 0.65 V (BEDOT-MOB) vs Ag/AgCl, consistent with that of previously studied BEDOT type monomers, 34,35 as a result of BEDOT's electron

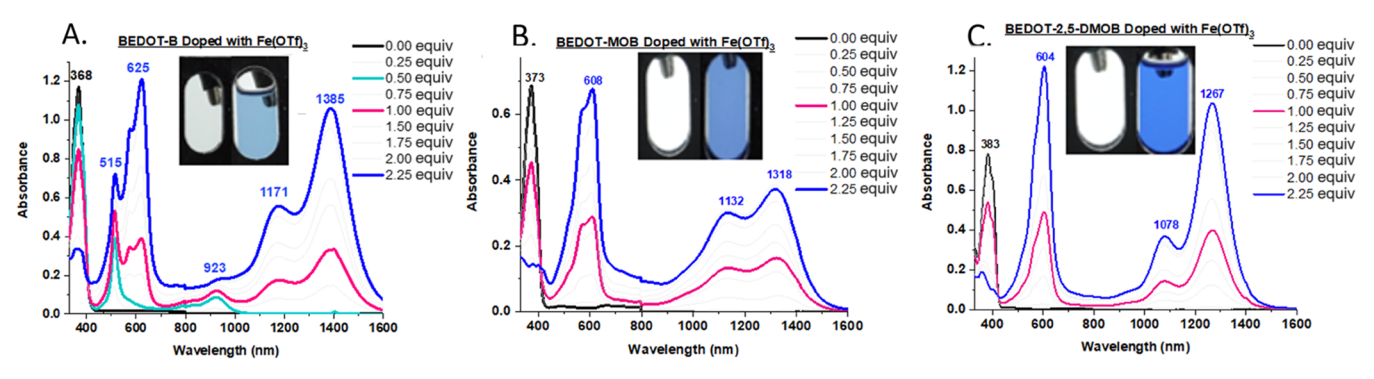


**Figure 9.** Evolution of UV–vis spectra of oxidatively doped molecules of (A) BEDOT-B, (B) BEDOT-MOB, and (C) BEDOT-2,5-DMOB using  $Fe(OTf)_3$  as the dopant in 250  $\mu$ M dichloromethane solution.

donation into the ring system (Figure S4B). Moreover, the additional EDOT in these three-ring chromophores decreases the first oxidation potential by at least 150 mV relative to the bi-aryl ACE molecules previously studied. This characteristic will be important and favorable when considering these molecules' potential deployment in low-voltage-driven ECDs. The peak-to-peak ( $\Delta E_{1-2}$ ) separation between the dominant oxidation waves decreases as the molecule becomes more electron-rich. To illustrate,  $\Delta E_{1-2}$  are 140, 130, and 120 mV for BEDOT-B, BEDOT-MOB, and BEDOT-2,5-DMOB, respectively. This observation indicates that the energy required to introduce a second positive charge to the molecule is less for BEDOT-2,5-DMOB than in BEDOT-B; hence, the *para*-methoxy groups likely aid in stabilizing a second charge.

Chemical and Electrochemical Generation of Radical Cation. Solution chemical oxidation measurements were conducted on the chromophores using iron(III) trifluoromethanesulfonate (Fe(Otf)<sub>3</sub>) as the oxidizing dopant ( $E_{1/2} = -0.2$  to -0.1 V vs Ag/Ag<sup>+</sup>)<sup>36</sup> in DCM to elucidate the shape and position of the radical cation absorbance. Relative to other common oxidizing agents, such as silver(I) hexafluorophosphate (AgPF<sub>6</sub>), Fe(Otf)<sub>3</sub> was previously shown to be an effective agent towards generating the oxidized species. <sup>12,36</sup>

The incremental addition of dopant equivalence demonstrated in Figure 9 led to a depletion of the neutral absorbance and a gradual increase in absorbance at longer wavelengths as charged states were generated. Comparing the three systems, BEDOT-B shows two absorbance bands in the HE region at  $\lambda_{\rm max}$  = 515 and 625 nm, whereas **BEDOT-MOB** ( $\lambda_{\rm max}$  = 608 nm) and BEDOT-2,5-DMOB ( $\lambda_{max}$  = 604 nm) have only a single peak. As mentioned in the calculations above, the  $S_{\alpha} \rightarrow$  $L_{\alpha}$  excited-state electronic transition is assigned to the growth of the radical cation HE peak. The strong absorption intensity is also supported by the high f values (near unity) calculated for this band. BEDOT-B has two distinct bands in the LE region at 1170 and 1385 nm with a small shoulder peak at ~920 nm (Figure 9A). BEDOT-MOB also has two absorbance peaks but differing from BEDOT-B, these peaks share closer in intensity at 1132 and 1318 nm (Figure 9B). BEDOT-2,5-DMOB displays two LE absorbance peaks that exhibit different intensities, with the stronger absorbance at 1267 nm and the weaker transition at 1078 nm.

Demonstrated through these observations, these electronrich BEDOT-X molecules all display LE absorbance in the NIR region, which leaves a single dominant transition in the visible. As illustrated by the pictures of the neutral and doped solutions, these chromophores switch from clear to various hues of blue upon oxidation. Hence, color vibrancy or saturation can be fine-tuned for the charged states in electrochromic applications.

Finally, Figure 10A shows an expanded view of the HE band for the chromophores. Overall, the absorbance bands for

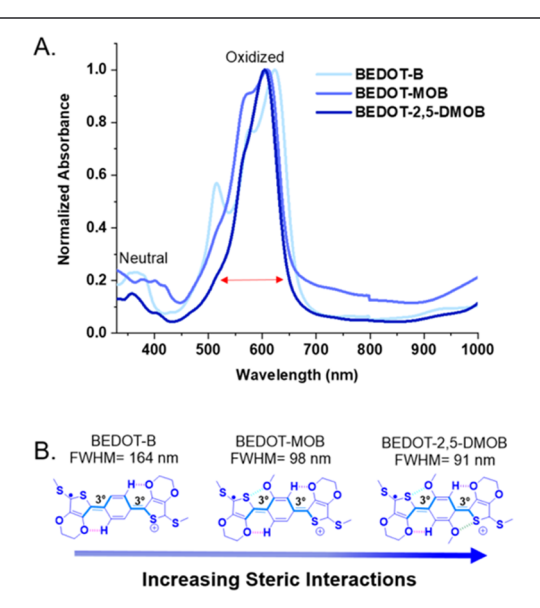
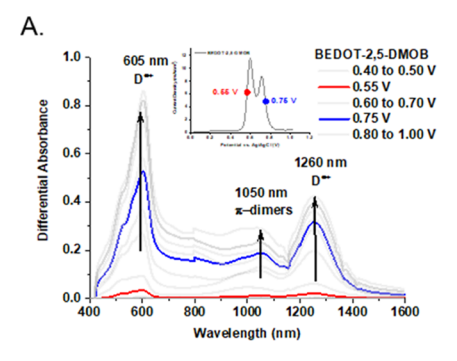


Figure 10. (A) Absorbance spectra of BEDOT-X radical cation species within the visible region. (B) Chemical structures of BEDOT-X in the radical cation forms. Their calculated dihedral angles and steric interactions (O···S, O···H, and O···O) are also shown. The associated full width at half-maximum (FWHM) HE values are listed above the structures.

oxidized BEDOT-2-5-DMOB are the most narrow in shape relative to the other two chromophores with a full width at half-maximum approximation (FWHM) of ca. 91 nm, which is backed up in comparison with the experimental and calculated spectra in Figure S5. While the  $\lambda_{\rm max}$  of these oxidized chromophores are nearly identical, the shape of their curves is sufficiently different, as evidenced by the large difference in their FWHM (~70 nm difference between BEDOT-B and BEDOT-2,5-DMOB), to impart variations in the colors of these states (Figure S6).

To gain further insight into the above observation, Figure 10B shows the quinoidal forms of the oxidized species, their respective calculated dihedral angles, and atom—atom interactions. The symmetric O···S interactions in BEDOT-2,5-DMOB lock the molecule into a planar conformation, thus possibly suppressing competing geometric configurations. In



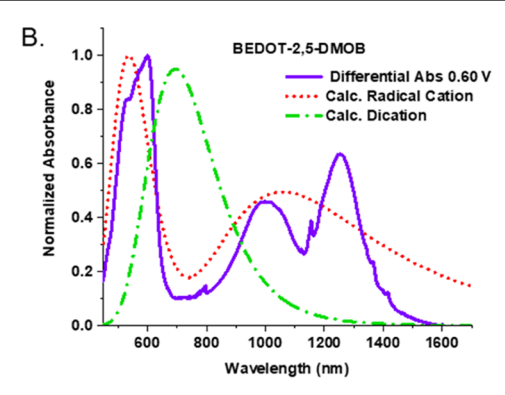


Figure 11. (A) Differential spectroelectrochemistry of BEDOT-2,5-DMOB. Inset: DPV scan showing respective potentials for monitoring the oxidized species. (B) Simulated spectra of oxidized species overlapped with normalized spectroelectrochemical spectra of BEDOT-2,5-DMOB at 1.0 V vs Ag/AgCl.

comparison, **BEDOT-MOB** lacks the second O···S interaction, and therefore has greater rotational freedom to access more excited-state conformations. Finally, **BEDOT-B** with only O··· H interactions present has the most twisted conformation out of the three, hence the greatest number of possible excited-state geometries. Therefore, as the number of favorable steric interactions increases (O···S), the radical cation becomes more stable, giving rise to narrow absorbance bands.

Next, spectroelectrochemistry and dication spectra simulations were employed to further evaluate the radical cation's optical properties and the possible presence of dication species. All measurements were done on each chromophore at 250  $\mu$ M concentration in a TBAPF<sub>6</sub>/DCM electrolyte solution using a Pt mesh working electrode, Pt flag counter electrode, and Ag/AgCl reference electrode. Each spectrum was recorded in 50 mV increments starting from 0.0 to 1.0 V vs Ag/AgCl. Before recording a spectrum, the potential was held for 120 s to ensure equilibrium color density was reached. Figure 11 shows the spectroelectrochemical absorption spectra of BEDOT-2,5-DMOB.

Following a previous procedure, the spectra were plotted as a function of differential absorbance to distinguish absorption peaks associated with the oxidized species, where the neutral absorbance was subtracted from the oxidized spectra (Figures S7-S9).<sup>37</sup> The inset in the figure displays the DPV of **BEDOT-2,5-DMOB** with the two oxidation peaks,  $E^{\text{ox1}} = 0.60$ V and  $E^{ox2} = 0.70$  V. At lower potentials, between 0.40 and 0.60 V, the absorbance peaks at 605 and 1260 nm began to grow in concurrence, which suggests that both peaks are associated with the formation of the radical cation. At higher potentials, >0.60 V corresponding to the second oxidation peak, a third absorbance band at 1050 nm becomes more prominent. We hypothesized that the third absorbance peak was associated with the formation of dication species; however, due to the small peak-to-peak separation in the DPV, an isolated spectrum of the possible dication could not be resolved.

Figure 11B shows the simulated radical cation and dication overlaid with the normalized differential absorbance spectrum taken at 0.6 V. The calculations reveal that the dication absorption (dashed green lines) should be significantly more blue-shifted than the observed experimental peak, suggesting that the peak at 1050 nm may not be the formation of dications (Figure 11B). Based on previous work and observations on similar  $\pi$ -conjugated systems,  $^{27,37-39}$  it is

more likely that the peak at 1050 nm is associated with the formation of  $\pi$ -dimers formed from radical cations.

To further emphasize this point, Nielsen et al. made similar observations through a UV-vis temperature-dependent study, where they found in the oxidized state of a thiophene/ ethylenedioxythiophene/phenylene (TPEEPT) oligomer, the radical cation coexists with the  $\pi$ -dimers at room temperature. Also, as the temperature decreases, the equilibrium shifts from the radical cation toward the dimeric species.<sup>36</sup> They also noted that a stronger oxidizing dopant nitrosonium hexafluorophosphate was needed to reach the dication state. Upon further oxidation using the stronger dopant, Nielsen observed that the absorption bands associated with the radical cation and  $\pi$ -dimer species disappeared, while the dication absorption peak grew in between the other two bands. Based on these previous observations, our choice of a weaker chemical oxidant, and the calculated/experimental spectra overlay, these results are consistent with the absorbance peak at 1050 nm shown in Figure 11 to be due to the formation of  $\pi$ -dimer species. While the identification of the  $\pi$ -dimer peak is important, we should also highlight that its absorption remains in the NIR region. Thus, in terms of the chromophore's electrochromic properties, the formation of these species does not interfere with the ACE's colored state.

Finally, the CIELAB (International Commission on Illumination  $L^*a^*b^*$ ) color space was used to quantify the hue and saturation of the electrochromes as they were converted from their colorless states to their colored states via solution oxidation. The  $a^*b^*$  plots are shown in Figure S10, where a quantitative change in color was observed upon gradual chemical oxidation as calculated from the UV—vis absorbance spectra of the neutral and doped solutions. In short, all three chromophores exhibited various saturation states of blue.

Summary and Perspective. In summary, seven all-donor thioalkyl-substituted bis (3,4-ethylenedioxythiophene)-1,4-phenylene, BEDOT-X molecules, were investigated as potential ACE chromophores. This work emphasizes the increasingly important role computations play in guiding synthetic efforts. TD-DFT calculations on the optical, geometric, and excited-state properties allowed for the generation of in-depth structure—property relationships of both the neutral and radical cation states of these seven molecules. Based on the analysis derived from calculations, three discrete  $\pi$ -conjugated, all-donor ter-heterocycle molecules based on BEDOT and alkoxyphenylene derivatives, BEDOT-B, BEDOT-MOB, and

BEDOT-2,5-DMOB were synthesized. UV—vis measurements of the chromophores in solution revealed that the neutral species display a  $\lambda_{\rm onset}$  of 425 nm or lower. The deviation is attributed to the Gaussian distribution fit around the lower-energy excitation wavelength. Despite this difference, strong spectral similarities between theory and experimental data of both the neutral and radical cations were observed.

The use of the BEDOT motif is influential in adding electron-rich character to the overall conjugated system and, along with the incremental addition of methoxy groups around the phenylene, oxidation potentials are low. Electrochemical measurements confirmed this by showing the three molecules oxidizing between 0.60 and 0.70 V vs Ag/AgCl. In comparison to previously studied ACE systems, the added electron-rich character ensures that the second absorbance band of the radical cation red-shifts into the NIR region. Theory also aided in understanding the electronic structure of the radical cations, giving rise to the two-band absorbance feature observed for all of the molecules studied here. While the position of the radical cation  $\lambda_{\text{max}}$  differs across the various ACE systems, we find that the peak in the HE region is attributed to the  $\alpha$  spin state (S<sub> $\alpha$ </sub>  $\rightarrow$  L<sub> $\alpha$ </sub>) transition, while the LE region is attributed to the  $\beta$ spin state  $(S_{\beta} \to L_{\beta})$  transition.

The position and number of the methoxy groups are influential in varying the steric interactions on the electrochromic properties of the chromophores. Comparisons of the molecule's crystal structures show an attractive O···S interaction between the methoxy group(s) and EDOT leading to near-planar conformations in BEDOT-MOB and BEDOT-2,5-DMOB. These geometric differences influenced the shape of the HE peak for the radical cation species. The UV-vis absorbance spectra for the chemically oxidized chromophores show that the width of the HE peak narrows as a function of planarity; BEDOT-B > BEDOT-MOB > BEDOT-2,5-DMOB. In general, all three radical cations display a transmission window between 400 and 450 nm giving rise to blue hues. BEDOT-2,5-DMOB displayed the narrowest peak and had the deepest transmission window, thus yielding the most vibrant color. These observations highlight the subtle strategy of using steric interactions to control the radical cation's color, hue, and saturation independent of the neutral absorbance.

Finally, this investigation also contributes to the design paradigm for developing new ACE materials. In comparison to previous systems, the radical cation absorbance of the BEDOT-X ACE family is more red-shifted, which allows for the transmission of low-energy light leading to the creation of blue colors, and ultimately expanding the color pallete (from red, green, and yellow) for the growing ACE class. Adding to the framework of using the electron-rich character to access different color spaces, we further show steric interactions' utility to fine-tune color vibrancy.

With respect to  $\pi$ -conjugated electrochromic polymers, which have the advantages of being highly processible through a variety of methods (ink jetting, blade-coating, spray coating, etc.) and if blended with other electrochromic polymers can create different colors, these ACE molecules are not compatible with the colorful class of cathodically coloring polymers. This mismatch stems from their different material properties (cathodic vs anodic, molecular adsorption vs film, polymer vs molecule). Although cathodically coloring electrochromic polymers achieve a variety of colored states, they are still plagued with the absorption of light in their transmissive

state. This issue is minimized, and in some cases, eliminated through the ACE design, therefore opening opportunities for the development of a full set of clear to colored switching organic electrochromic molecules.

#### EXPERIMENTAL DETAILS

**Instrumentation.** All reactions were carried under Ar atmosphere. Anhydrous toluene, tetrahydrofuran, and dichloromethane were taken from a solvent purification system. NMR spectra were collected on Varian Mercury Vx (300 MHz <sup>1</sup>H, 75 MHz <sup>13</sup>C) or Bruker Avance IIIHD 500 (500 MHz <sup>1</sup>H, 126 MHz <sup>13</sup>C). Spectra were processed using MestReNova V6.0 and referenced to residual protonated solvent signals (CDCl<sub>3</sub>: <sup>1</sup>H 7.26 ppm, <sup>13</sup>C 77.16; DMSO-d<sub>6</sub>: <sup>1</sup>H 2.50 ppm, <sup>13</sup>C 39.52 ppm; CD<sub>3</sub>OD: <sup>1</sup>H 3.31 ppm, <sup>13</sup>C 49.00 ppm). The solvent peak used as the internal reference is labeled in each spectrum as its deuterated parent solvent. Accurate mass spectra were collected by the Bioanalytical Mass Spectrometry Facility at Georgia Tech on a Micromass Autospec M (EI). Both electron spray ionization (ESI) and high-resolution mass spectra (HRMS) were taken on a Waters Autospec M Three Sector Tandem mass spectrometer. Colorimetry measurements were obtained using Star-Tek colorimetry software using a D50 illuminant, 2-degree observer, and the  $L^*a^*b^*$  color space. Absorption spectra measurements were performed using an Agilent Cary 5000 UV-vis-NIR dual-beam spectrophotometer.

**Electrochemistry.** All electrochemical measurements were done in an EG&G Princeton Applied Research 273A potentiostat/galvanostat under CorrWare control. Solution electrochemistry was performed in a three-electrode cell using Ag/AgCl reference electrode, Pt flag counter electrode, and 0.02 cm² Pt button working electrode or  $1 \times 1$  cm² Pt mesh for optically transparent thin-layer electrode (OTTLE) measurements with tetrabutylammonium hexafluorophosphate (TBAPF<sub>6</sub>) as the supporting electrolyte in dichloromethane at 0.5 M concentration. Cyclic voltammetry (CV) was performed at a 50 mV s⁻¹ scan rate, and differential pulse voltammetry (DPV) was performed using a 2 mV step size, 80 ms step time, and 50 mV pulse amplitude. All voltammetry experiments were performed under constant argon flow. Ferrocene/ferrocenium (–5.12 V vs vacuum) was used as an internal standard calibrated against the Ag/AgCl reference electrode ( $E_{1/2} = 398$  mV).

Chemical Doping Measurements. All chemical doping experiments were performed in dichloromethane solutions. The solvent was degassed with at least three freeze—pump—thaw cycles and stored in a glovebox under light protection. The chemical oxidant, iron(III) trifluoromethanesulfonate (purchased from Millipore Sigma and used without further modification), was stored inside the glovebox. The experiment was conducted as previously described. <sup>1</sup>

Spectroelectrochemistry. Optical absorption spectra were collected at room temperature using an Agilent Cary 5000 UVvis-NIR spectrophotometer, in an OTTLE cuvette for solution electrochemical experiments. A constant gentle flow of argon was delivered to the spectrometer throughout all of the experiments. Spectroelectrochemistry was carried out using 0.5 mM TBAPF<sub>6</sub> as the supporting electrolyte in dichloromethane, Ag/AgCl reference electrode, and Pt button (OTTLE measurements). Spectral changes were monitored using the spectrophotometer. An EG&G Princeton Applied Research 263A using the CorrWare software package controlled the applied potential to the working electrode. A potential step of 50 mV was used with each potential maintained for 3 min before a UV-vis absorption spectrum was taken. Corresponding photographs of the electrochemical cells used in these experiments were taken in a light booth that was illuminated by a D50 (5000 K) lamp, using a Nikon D90 SLR camera with a Nikon 18-105 mm VR lens and are reported without further manipulation beyond photograph cropping.

**Solution Colorimetry.** Calculated  $L^*a^*b^*$  values for the neutral states are as follows: **BEDOT-2,5-DMOB** (100, 0, 1), **BEDOT-MOB** (99, 0, 1), and **BEDOT-B** (99, 0, 0), indicating they are color-neutral and fully transmissive in their unoxidized states. In contrast to the neutral states' nearly identical  $L^*a^*b^*$  values, the oxidized species

color coordinates show distinct variations. As shown by the tracking in Figure S10A and summarized in Table S9, all three chromophores have negative  $b^*$  values ranging from -40 to -64 and positive  $a^*$ values ranging from 14 to 38 when fully oxidized. The large negative b\* coordinates position the chromophores in the blue color quadrant, while the positive a\* values indicate that varying degrees of red contribute to the hue. For example, BEDOT-B ( $a^* = 38$ ) and **BEDOT-2,5-DMOB** ( $a^* = 30$ ) radical cations have the highest  $a^*$ values. According to its CIELAB coordinates, these chromophores can be identified as having a medium slate blue or light blue color. Still staying in the blue quadrant ( $b^* = -40$ ), but decreasing the  $a^*$ value to 14, BEDOT-MOB can be classified as a ciel blue or sky-blue color. These colors are comparable to the popular 1,1'-disubstituted-4-4'-bipyridinium salts (viologens), which also exhibit a blue color in the radical cation form. Shown in Figure S10B, joining forces with the previously studied chromophores, ACE1-4 (oxidized species appear as red, green, and yellow), our work demonstrates the successful expansion of the color palette for the underdeveloped class of discrete anodic coloring materials.

#### ASSOCIATED CONTENT

#### Supporting Information

The Supporting Information is available free of charge at https://pubs.acs.org/doi/10.1021/acs.chemmater.2c02054.

Experimental and computational results for photophysical properties; calculated molecular structures (neutral and cation radical); electronic spectra; cyclic voltammetry; differential pulse voltammetry; spectroelectrochemistry; chemical doping; solution colorimetry; synthetic details; and the Gaussian data for all BEDOT-X molecules. (PDF

CIF's for BEDOT-2,5-DMOB, deposition number 2182339 with VRF (CIF) and BEDOT-MOB deposition number 2182338 (CIF) are filed with the Cambridge Crystallographic Data Centre (CCDC). deposition number 2182339 with VRF (CIF)

BEDOT-MOB deposition number 2182338 (CIF)

#### AUTHOR INFORMATION

#### **Corresponding Author**

John R. Reynolds — School of Chemistry and Biochemistry, Georgia Institute of Technology, Atlanta, Georgia 30332, United States; School of Materials Science and Engineering, Center for Organic Photonics and Electronics, Georgia Tech Polymer Network, Georgia Institute of Technology, Atlanta, Georgia 30332, United States; orcid.org/0000-0002-7417-4869; Email: Reynolds@chemistry.gatech.edu

#### Author

- Linda Nhon School of Chemistry and Biochemistry, Georgia Institute of Technology, Atlanta, Georgia 30332, United States
- Simone L. Tennyson School of Chemistry and Biochemistry, Georgia Institute of Technology, Atlanta, Georgia 30332, United States
- Mason W. Butt Department of Chemistry/Biochemistry, University of North Georgia, Dahlonega, Georgia 30597, United States
- John Bacsa X-ray Crystallography Center, Department of Chemistry, Emory University, Atlanta, Georgia 30322, United States
- Aimée L. Tomlinson Department of Chemistry/ Biochemistry, University of North Georgia, Dahlonega,

Georgia 30597, United States; o orcid.org/0000-0002-6953-4970

Complete contact information is available at: https://pubs.acs.org/10.1021/acs.chemmater.2c02054

#### Notes

The authors declare no competing financial interest.

#### ACKNOWLEDGMENTS

Funding from the Air Force Office of Scientific Research (FA9550-18-1-0184, FA9550-21-1-0420, and FA9550-18-1-0034) and supercomputer access through the National Science Foundation's Extreme Science and Engineering Discovery Environment (NSF XSEDE, DMR 160146) are acknowledged. The authors also thank Dr. Anna Österholm, Dr. Eric Shen, and Dr. Justine Wagner for their thoughtful input, warm candor, and last-minute help in getting this manuscript to the finish line.

#### **■** REFERENCES

- (1) Hirata, S.; Head-Gordon, M. Time-dependent density functional theory for radicals: An improved description of excited states with substantial double excitation character. *Chem. Phys. Lett.* **1999**, 302, 375–382.
- (2) Jacquemin, D.; Wathelet, V.; Perpète, E. A.; Adamo, C. Extensive TD-DFT Benchmark: Singlet-Excited States of Organic Molecules. *J. Chem. Theory Comput.* **2009**, *5*, 2420–2435.
- (3) Schleder, G. R.; Padilha, A. C. M.; Acosta, C. M.; Costa, M.; Fazzio, A. From DFT to Machine Learning: Recent Approaches to Materials Science A Review. *J. Phys.: Mater.* **2019**, *2*, No. 032001.
- (4) Shao, Y.; Mei, Y.; Sundholm, D.; Kaila, V. R. I. Benchmarking the Performance of Time-Dependent Density Functional Theory Methods on Biochromophores. *J. Chem. Theory Comput.* **2020**, *16*, 587–600.
- (5) Chen, G.; Shen, Z.; Iyer, A.; Ghumman, U. F.; Tang, S.; Bi, J.; Chen, W.; Li, Y. Machine-Learning-Assisted De Novo Design of Organic Molecules and Polymers: Opportunities and Challenges. *Polymers* **2020**, *12*, No. 163.
- (6) Santos, G. C.; Roldao, J. C.; Shi, J.; Milián-Medina, B.; da Silva-Filho, L. C.; Gierschner, J. Combined Spectroscopic and TD-DFT Analysis to Elucidate Substituent and Acidochromic Effects in Organic Dyes: A Case Study on Amino- versus Nitro-Substituted 2,4-Diphenylquinolines. *ChemPhysChem* **2020**, *21*, 1797–1804.
- (7) Deogratias, G.; Seriani, N.; Pogrebnaya, T.; Pogrebnoi, A. Tuning Optoelectronic Properties of Triphenylamine Based Dyes through Variation of Pi-Conjugated Units and Anchoring Groups: A DFT/TD-DFT Investigation. *J. Mol. Graphics Modell.* **2020**, *94*, No. 107480.
- (8) Mathiyalagan, A.; Manimaran, K.; Muthu, K.; Rajakantham, M. Density Functional Theory Study on the Electronic Structures and Spectral Properties of 3,5-Dimethylanisole Dye Sensitizer for Solar Cell Applications. *Results Chem.* **2021**, *3*, No. 100164.
- (9) Kiely, E.; Zwane, R.; Fox, R.; Reilly, A. M.; Guerin, S. Density Functional Theory Predictions of the Mechanical Properties of Crystalline Materials. *CrystEngComm* **2021**, 23, 5697–5710.
- (10) Kzar Al-Masoodi, K. O.; Rafiq, I.; Assyry, A. E.; Derouiche, A. DFT/TD-DFT Study of Donorπ-Acceptor Organic Dye models contained Triarylamine for an Efficient Dye-Sensitized Solar Cell. *J. Phys.: Conf. Ser.* **2021**, *1963*, No. 012012.
- (11) Nakata, A.; Bowler, R. D.; Miyazaki, T. Large-Scale DFT Methods for Calculations of Materials with Complex Structures. *J. Phys. Soc. Jpn.* **2022**, *91*, No. 091011.
- (12) Christiansen, D. T.; Tomlinson, A. L.; Reynolds, J. R. New Design Paradigm for Color Control in Anodically Coloring Electrochromic Molecules. *J. Am. Chem. Soc.* **2019**, *141*, 3859–3862.

- (13) Gillaspie, D. T.; Tenent, R. C.; Dillon, A. C. Metal-Oxide Films for Electrochromic Applications: Present Technology and Future Directions. *J. Mater. Chem.* **2010**, 20, 9585–9592.
- (14) Zhai, Y.; Li, Y.; Zhu, Z.; Zhu, C.; Du, D.; Lin, Y. Self-Driven Multicolor Electrochromic Energy Storage Windows Powered by a "Perpetual" Rechargeable Battery. ACS Appl. Mater. Interfaces 2019, 11, 48013–48020.
- (15) Ke, Y.; Chen, J.; Lin, G.; Wang, S.; Zhou, Y.; Yin, J.; Lee, P. S.; Long, Y. Smart Windows: Electro-, Thermo-, Mechano-, Photochromics, and Beyond. *Adv. Energy Mater.* **2019**, *9*, No. 1902066.
- (16) Xia, X.; Ku, Z.; Zhou, D.; Zhong, Y.; Zhang, Y.; Wang, Y.; Huang, M. J.; Tu, J.; Fan, H. J. Perovskite Solar Cell Powered Electrochromic Batteries for Smart Windows. *Mater. Horiz.* **2016**, 3, 588–595.
- (17) Mortimer, R. J.; Dyer, A. L.; Reynolds, J. R. Electrochromic Organic and Polymeric Materials for Display Applications. *Displays* **2006**, *27*, 2–18.
- (18) Bae, S.; Kim, H.; Lee, Y.; Xu, X.; Park, J.-S.; Zheng, Y.; Balakrishnan, J.; Lei, T.; Ri Kim, H.; Song, Y. I.; et al. Roll-To-Roll Production of 30-Inch Graphene Films for Transparent Electrodes. *Nat. Nanotechnol.* **2010**, *5*, 574–578.
- (19) Xiong, J.; Lin, M.-F.; Wang, J.; Gaw, S. L.; Parida, K.; Lee, P. S. Wearable All-Fabric-Based Triboelectric Generator for Water Energy Harvesting. *Adv. Energy Mater.* **2017**, *7*, No. 1701243.
- (20) Cao, K.; Shen, D. E.; Österholm, A. M.; Kerszulis, J. A.; Reynolds, J. R. Tuning Color, Contrast, and Redox Stability in High Gap Cathodically Coloring Electrochromic Polymers. *Macromolecules* **2016**, *49*, 8498–8507.
- (21) Beaujuge, P. M.; Reynolds, J. R. Color Control in  $\pi$ -Conjugated Organic Polymers for Use in Electrochromic Devices. *Chem. Rev.* **2010**, *110*, 268–320.
- (22) Zhou, D.; Xie, D.; Xia, X.; Wang, X.; Gu, C.; Tu, J. All-Solid-State Electrochromic Devices Based On WO3||NiO Films: Material Developments and Future Applications. *Sci. China Chem.* **2017**, *60*, 3–12.
- (23) Madasamy, K.; Velayutham, D.; Suryanarayanan, V.; Kathiresan, M.; Ho, K.-C. Viologen-Based Electrochromic Materials and Devices. *J. Mater. Chem. C* **2019**, *7*, 4622–4637.
- (24) Jackson, N. E.; Savoie, B. M.; Kohlstedt, K. L.; Olvera de la Cruz, M.; Schatz, G. C.; Chen, L. X.; Ratner, M. A. Controlling Conformations of Conjugated Polymers and Small Molecules: The Role of Nonbonding Interactions. *J. Am. Chem. Soc.* **2013**, *135*, 10475–10483.
- (25) Wheeler, D. L.; Rainwater, L. E.; Green, A. R.; Tomlinson, A. L. Modeling electrochromic poly-dioxythiophene-containing materials through TDDFT. *Phys. Chem. Chem. Phys.* **2017**, *19*, 20251–20258.
- (26) Png, R.-Q.; Ang, M. C. Y.; Teo, M.-H.; Choo, K.-K.; Tang, C. G.; Belaineh, D.; Chua, L.-L.; Ho, P. K. H. Madelung and Hubbard interactions in polaron band model of doped organic semiconductors. *Nat. Commun.* **2016**, *7*, No. 11948.
- (27) Sahalianov, I.; Hynynen, J.; Barlow, S.; Marder, S. R.; Müller, C.; Zozoulenko, I. UV-to-IR Absorption of Molecularly p-Doped Polythiophenes with Alkyl and Oligoether Side Chains: Experiment and Interpretation Based on Density Functional Theory. *J. Phys. Chem. B* **2020**, *124*, 11280–11293.
- (28) Winkler, S.; Amsalem, P.; Frisch, J.; Oehzelt, M.; Heimel, G.; Koch, N. Probing the Energy Levels in Hole-Doped Molecular Semiconductors. *Mater. Horiz.* **2015**, *2*, 427–433.
- (29) Zhang, W.; Zhu, W.; Liang, W.; Zhao, Y.; Nelsen, S. F. Ab Initio Calculations on the Intramolecular Electron Transfer Rates of a Bis(hydrazine) Radical Cation. *J. Phys. Chem. B* **2008**, *112*, 11079–11086.
- (30) Nelsen, S. F.; Blackstock, S. C.; Kim, Y. Estimation of Inner Shell Marcus Terms for Amino Nitrogen Compounds by Molecular Orbital Calculations. *J. Am. Chem. Soc.* **1987**, *109*, 677–682.
- (31) Ashassi-Sorkhabi, H.; Salehi-Abar, P. How the change of OMe substituent position affects the performance of spiro-OMeTAD in neutral and oxidized forms: theoretical approaches. *RSC Adv.* **2018**, *8*, 18234–18242.

- (32) Marques, G.; Leswing, K.; Robertson, T.; Giesen, D.; Halls, M. D.; Goldberg, A.; Marshall, K.; Staker, J.; Morisato, T.; Maeshima, H.; et al. De Novo Design of Molecules with Low Hole Reorganization Energy Based on a Quarter-Million Molecule DFT Screen. *J. Phys. Chem. A* **2021**, *125*, 7331–7343.
- (33) Sotzing, G. A.; Reynolds, J. R.; Steel, P. J. Electrochromic Conducting Polymers via Electrochemical Polymerization of Bis(2-(3,4-ethylenedioxy)thienyl) Monomers. *Chem. Mater.* **1996**, *8*, 882–889
- (34) Sotzing, G. A.; Reddinger, J. L.; Reynolds, J. R.; Steel, P. J. Redox Active Electrochromic Polymers from Low Oxidation Monomers containing 3,4-Ethylenedioxythiophene (EDOT). *Synth. Met.* **1997**, *84*, 199–201.
- (35) Irvin, J. A.; Reynolds, J. R. Low-Oxidation-Potential Conducting Polymers: Alternating Substituted Para-Phenylene and 3,4-Ethylenedioxythiophene Repeat Units. *Polymer* **1998**, *39*, 2339—2347.
- (36) Pittelli, S. L.; Shen, D. E.; Österholm, A. M.; Reynolds, J. R. Chemical Oxidation of Polymer Electrodes for Redox Active Devices: Stabilization through Interfacial Interactions. *ACS Appl. Mater. Interfaces* **2018**, *10*, 970–978.
- (37) Teran, N. B.; Reynolds, J. R. Discrete Donor–Acceptor Conjugated Systems in Neutral and Oxidized States: Implications toward Molecular Design for High Contrast Electrochromics. *Chem. Mater.* **2017**, *29*, 1290–1301.
- (38) Nielsen, C. B.; Angerhofer, A.; Abboud, K. A.; Reynolds, J. R. Discrete Photopatternable  $\pi$ -Conjugated Oligomers for Electrochromic Devices. *J. Am. Chem. Soc.* **2008**, *130*, 9734–9746.
- (39) Christiansen, D. T.; Wheeler, D. L.; Tomlinson, A. L.; Reynolds, J. R. Electrochromism of Alkylene-Linked Discrete Chromophore Polymers with Broad Radical Cation Light Absorption. *Polym. Chem.* **2018**, *9*, 3055–3066.
- (40) Tkalcic, M.; Tasic, J. F.Colour Spaces: Perceptual, Historical and Applicational Background; IEEE, 2003; Vol. 1.

### **□** Recommended by ACS

Intersystem Crossing in Acceptor-Donor-Acceptor Type Organic Photovoltaic Molecules Promoted by Symmetry Breaking in Polar Environments

Ziran Liu, Chunfeng Zhang, et al.

OCTOBER 28, 2022

THE JOURNAL OF PHYSICAL CHEMISTRY LETTERS

READ 🗹

Uncovered Effects of thieno[2,3-b]thiophene Substructure in a Tetrathienoacene Backbone: Reorganization Energy and Intermolecular Interaction

Kiseki Kanazawa, Kazuo Takimiya, et al.

DECEMBER 12, 2022

CHEMISTRY OF MATERIALS

READ 🗹

Influence of End-Capped Modifications in the Nonlinear Optical Amplitude of Nonfullerene-Based Chromophores with a  $D-\pi-A$  Architecture: A DFT/TDDFT Study

Muhammad Khalid, Aman Ullah, et al.

JUNE 23, 2022

ACS OMEGA

READ 🗹

Reconsidering the Roles of Noncovalent Intramolecular "Locks" in  $\pi$ -Conjugated Molecules

Chamikara Karunasena, Chad Risko, et al.

NOVEMBER 15, 2021

CHEMISTRY OF MATERIALS

READ 🗹

Get More Suggestions >